Contents lists available at ScienceDirect

Petroleum Science

journal homepage: www.keaipublishing.com/en/journals/petroleum-science

Original Paper

Gas prediction in tight sandstones based on the rock-physics-derived seismic amplitude variation versus offset method

Han Jin, Cai Liu, Zhi-Qi Guo [*]

College of Geoexploration Science and Technology, Jilin University, Changchun, 130026, Jilin, China

ARTICLE INFO

ABSTRACT

Estimating gas enrichments is a key objective in exploring sweet spots within tight sandstone gas reservoirs. However, the low sensitivity of elastic parameters to gas saturations in such formations makes it a significant challenge to reliably estimate gas enrichments using seismic methods. Through rock physical modeling and reservoir parameter analyses conducted in this study, a more suitable indicator for estimating gas enrichment, termed the gas content indicator, has been proposed. This indicator is formulated based on effective fluid bulk modulus and shear modulus and demonstrates a clear positive correlation with gas content in tight sandstones. Moreover, a new seismic amplitude variation versus offset (AVO) equation is derived to directly extract reservoir properties, such as the gas content indicator and porosity, from prestack seismic data. The accuracy of this proposed AVO equation is validated through comparison with the exact solutions provided by the Zoeppritz equation. To ensure reliable estimations of reservoir properties from partial angle-stacked seismic data, the proposed AVO equation is reformulated within the elastic impedance inversion framework. The estimated gas content indicator and porosity exhibit favorable agreement with logging data, suggesting that the obtained results are suitable for reliable predictions of tight sandstones with high gas enrichments. Furthermore, the proposed methods have the potential to stimulate the advancement of other suitable inversion techniques for directly estimating reservoir properties from seismic data across various petroleum resources.

1. Introduction

Global natural gas production has been significantly enhanced by tight sandstones, which represent one of the primary unconventional hydrocarbon reservoirs. The foundation of high-quality tight sandstones lies in their high gas enrichment, with a sufficiently substantial gas accumulation being essential for the production capabilities of tight sandstone gas reservoirs. Hence, gas prediction assumes primary importance in the exploration and development of these reservoirs. However, tight sandstone gas reservoirs typically exhibit low porosity, low permeability, complex pore structures, and significant heterogeneity (Liu et al., 2019; Shu et al., 2021). The intricate elastic properties linked to gas saturations and porosities in tight sandstones make considerable challenges in achieving reliable gas predictions using seismic methods (Ren et al., 2014; Cui et al., 2017).

In petroleum reservoir fluid predictions, Smith and Gidlow (1987) employed weighted stacking schemes to estimate rock properties and identify gas presence. Fatti et al. (1994) introduced fluid indicator traces for gas detection based on seismic amplitude variation with offset (AVO) analysis and the mudrock line concept. Additionally, Goodway et al. (1997) emphasized the importance of elastic moduli over velocities and density for fluid detection, suggesting the use of Lamé impedance to distinguish reservoir fluid types. Quakenbush et al. (2006) further proposed Poisson's impedance as an indicator for hydrocarbon detection and porosity prediction.

Numerous researchers have delved into pore structure analysis using rock physics methods to enhance the precision of reservoir property identification (Gurevich et al., 2009; Glubokovskikh et al., 2016; Chen et al., 2023a, 2023b). Rock physics methods have been employed to identify fluids in tight gas sandstone reservoirs (Li et al., 2017; Yin et al., 2017). Several fluid indicators have been proposed based on different combinations of elastic parameters. Russell et al. (2003) proposed using the fluid term (ρf) as a fluid

* Corresponding author.
E-mail address: guozhiqi@jlu.edu.cn (Z.-Q. Guo).

discriminator, where ρ represents density and f denotes the Gassmann fluid factor. Additionally, Russell et al. (2006) introduced a three-term approximation of the AVO equation, incorporating the Gassmann fluid factor, shear modulus, and density. This approach offers a means to predict fluids using prestack seismic data. Zhang et al. (2010) claimed that the Gassmann fluid factor may lead to ambiguities in the pore fluid identification owing to the effect of porosity. To address this issue, numerous researchers have developed new linearized AVO approximations based on effective fluid bulk modulus and pertinent elastic properties (Yin and Zhang, 2014; Zong et al., 2015; Zhang, 2016; Zhang et al., 2017). Additionally, based on the analyses of the relations between reservoir properties and elastic parameters, Xu et al. (2014) contended that the parameter λ/V_{S} (where λ is the Lamé coefficient and V_{S} is the shear-wave velocity) exhibits sensitivity to gas and can enhance gas identification in tight sandstones. Huang et al. (2015) introduced a fluid indicator linked to $\beta^2 M$ for fluid identification, where β denotes the Biot coefficient and M is the term associated with the effects of fluids and pores. Wang et al. (2020) integrated deterministic and statistical rock physics approaches, introducing a joint posterior probability to discriminate fluids. The methodology enabled the extraction of high-precision elastic parameters from seismic data by employing the reflectivity method. In another study, Wang et al. (2022) introduced a novel fluid identification parameter known as the inclusion-based effective fluid modulus, which enhances fluid identification in tight gas-bearing reservoirs.

In addition to the studies on fluid indicators mentioned above, significant efforts have been dedicated to achieving direct inversion of reservoir parameters from seismic data. It was generally acknowledged that direct estimation of reservoir parameters from prestack seismic data can help mitigate accumulative errors. Zong et al. (2012) derived an approximate AVO equation for the direct estimation of compression and shear moduli, which was utilized to construct a fluid factor. Additionally, Yin et al. (2013) accomplished a direct estimation of Russell's fluid factor through Bayesian elastic impedance inversion. Their method offered a robust approach to fluid detection, enhancing reservoir fluid identification. Zong and Yin (2017) developed an AVO equation for the direct inversion of Young's and Poisson's impedances, demonstrating promise in lithology and fluid prediction for unconventional resources. Jia et al. (2018) introduced a generalized elastic impedance equation to estimate the gas-sensitive factor f/V_{S}. Moreover, Gao et al. (2019) devised a sensitive lithology indicator and an AVO equation for sandstone identification. Additionally, Zhang et al. (2020a) formulated a parameter to mitigate porosity influence in fluid detection. Zhang et al. (2020b) proposed an oil-porosity factor and established an AVO equation for characterizing oil-bearing reservoirs. Recently, leveraging the double-porosity Biot-Rayleigh model, Guo et al. (2022) developed a multi-objective seismic inversion method for direct estimation of petrophysical parameters. Chen et al. (2022) introduced a generalized elastic impedance equation to directly invert $V_{\mathrm{P}}/V_{\mathrm{S}}$, V_{P}, and ρ in gas-bearing carbonate reservoirs. In addition, by accounting for azimuthal variations in seismic signatures, Chen and Zong (2022) introduced stress-induced anisotropy factors. Ma et al. (2023) introduced an effective fluid indicator ($\beta K_{\mathrm{f}}/\varphi$) for hydrocarbon identification in titled transversely isotropic media, where K_{f} and φ represent the fluid bulk modulus and porosity, respectively.

In this study, the primary aim of this paper is to devise a method for accurate gas predictions using prestack seismic data. To accomplish this goal, a gas content indicator is first introduced based on rock physical modeling and reservoir parameter analyses

using well-log data. Subsequently, a seismic AVO equation that is parameterized by the gas content indicator and porosity is derived by incorporating rock physical relationships. An accuracy analysis of the proposed AVO equation is then conducted. Following that, the elastic impedance inversion scheme is employed utilizing the derived AVO equation to directly estimate the gas content indicator and porosity. Subsequently, the proposed method is applied to field data to estimate the gas content indicator and porosity in tight sandstone gas reservoirs. These results are then calibrated with logging data to assess the effectiveness of our approach. Additionally, the robustness and reliability of both direct and indirect methods are compared for estimating the gas content indicator.

2. Theory and methodology

2.1. A new AVO equation for direct estimation of reservoir properties

Murphy et al. (1991) proposed the formulas of velocities based on Gassmann's equation:

$$\rho V_{\mathrm{P}}^2 = K_{\mathrm{dry}} + \frac{4}{3}\mu + f \tag{1}$$

$$\rho V_{\mathrm{S}}^2 = \mu \tag{2}$$

$$f = \frac{\left(1 - \frac{K_{\mathrm{dry}}}{K_{\mathrm{s}}}\right)^2}{\frac{\varphi}{K_{\mathrm{f}}} + \frac{1-\varphi}{K_{\mathrm{s}}} - \frac{K_{\mathrm{dry}}}{K_{\mathrm{s}}^2}} \tag{3}$$

where V_{P}, V_{S}, and ρ represent the compressional wave velocity, shear wave velocity, and density, respectively, of the saturated rock. Also, K_{dry} denotes the bulk modulus of the dry rock, μ signifies the shear modulus of the rock skeleton, K_{s} stands for the bulk modulus of the solid grain, K_{f} represents the fluid bulk modulus, φ is the porosity, and f represents the fluid/porosity term.

Han and Batzle (2003) proposed the simplified form of the fluid/porosity term f as

$$f = K_{\mathrm{f}} G(\varphi) \tag{4}$$

where $G(\varphi) = \frac{(1 - K_{\mathrm{dry}}/K_{\mathrm{s}})^2}{\varphi}$.

Defining the factor F in Eq. (5):

$$F = \frac{1}{K_{\mathrm{f}}\mu} \tag{5}$$

Drawing upon Fatti's P-wave reflection coefficient equation (Fatti et al., 1994) in Eq. (6), a new AVO Equation was established in Eq. (7):

$$R_{\mathrm{PP}}(\theta) = \frac{(1 + \tan^2\theta)}{2}\frac{\Delta I_{\mathrm{P}}}{I_{\mathrm{P}}} - \frac{4}{\gamma_{\mathrm{sat}}^2}\sin^2\theta\frac{\Delta I_{\mathrm{S}}}{I_{\mathrm{S}}} - \left(\frac{\tan^2\theta}{2} \right.$$
$$\left. - \frac{2}{\gamma_{\mathrm{sat}}^2}\sin^2\theta\right)\frac{\Delta\rho}{\rho} \tag{6}$$

$$R_{PP}(\theta) = -\frac{(1+\tan^2\theta)\left(\gamma_{sat}^2 - \gamma_{dry}^2\right)}{4\gamma_{sat}^2}\frac{\Delta F}{F} - \frac{(1+\tan^2\theta)\left(\gamma_{sat}^2 - 2\gamma_{dry}^2\right) + 8\sin^2\theta}{2\gamma_{sat}^2}\frac{\Delta(\varphi I_S)}{\varphi I_S}$$
$$+ \left[\frac{(1+\tan^2\theta)\left(\gamma_{sat}^2 - \gamma_{dry}^2\right) + 4\sin^2\theta}{2\gamma_{sat}^2} - \frac{\tan^2\theta}{2}\right]\frac{\Delta\rho}{\rho}$$
$$+ \frac{(1+\tan^2\theta)\left(3\gamma_{sat}^2 - 5\gamma_{dry}^2\right) + 16\sin^2\theta}{4\gamma_{sat}^2}\frac{\Delta\varphi}{\varphi} \tag{7}$$

In this newly developed AVO equation, $R_{PP}(\theta)$ is parameterized by the reflectivity terms $\Delta F/F$, $\Delta(\varphi I_S)/(\varphi I_S)$, $\Delta\rho/\rho$, and $\Delta\varphi/\varphi$. Derivations from Eqs. (6) and (7) are given in Appendix A. Eq. (7) provides a method for direct estimations of reservoir properties (such as gas content indicator F and porosity φ) using prestack seismic data. The proposed factor F serves as a valuable tool for discerning gas content, exhibiting greater sensitivity in identifying tight sandstones with medium to high gas saturation compared to the fluid bulk modulus (K_f).

2.2. Elastic impedance inversion scheme by utilizing the proposed AVO equation

Connolly (1999) proposed the elastic impedance inversion method, which establishes the relationship between $R_{PP}(\theta)$ and the elastic impedance $EI(\theta)$ as follows:

$$R_{PP}(\theta) = \frac{EI_2(\theta) - EI_1(\theta)}{EI_2(\theta) + EI_1(\theta)} = \frac{1}{2}\frac{\Delta EI(\theta)}{\overline{EI}(\theta)} \approx \frac{1}{2}\Delta\ln[EI(\theta)] \tag{8}$$

where $EI_1(\theta)$ and $EI_2(\theta)$ are the elastic impedances of the upper and lower media, respectively, across a subsurface interface. In addition, $\Delta EI(\theta)$ and $\overline{EI}$ denotes the difference and average, respectively, of the upper and lower impedances across the interface.

Based on the relation presented in Eq. (8), the $R_{PP}(\theta)$ in Eq. (7) can be expressed as:

$$EI(\theta) = F^{a(\theta)}(\varphi I_S)^{b(\theta)}\rho^{c(\theta)}\varphi^{d(\theta)} \tag{9}$$

where

$$a(\theta) = -\frac{(1+\tan^2\theta)\left(\gamma_{sat}^2 - \gamma_{dry}^2\right)}{2\gamma_{sat}^2} \tag{10}$$

$$b(\theta) = -\frac{(1+\tan^2\theta)\left(\gamma_{sat}^2 - 2\gamma_{dry}^2\right) + 8\sin^2\theta}{\gamma_{sat}^2} \tag{11}$$

$$c(\theta) = \left[\frac{(1+\tan^2\theta)\left(\gamma_{sat}^2 - \gamma_{dry}^2\right) + 4\sin^2\theta}{\gamma_{sat}^2} - \tan^2\theta\right] \tag{12}$$

$$d(\theta) = \left[\frac{(1+\tan^2\theta)\left(3\gamma_{sat}^2 - 5\gamma_{dry}^2\right) + 16\sin^2\theta}{2\gamma_{sat}^2}\right] \tag{13}$$

According to Whitecombe et al. (2002), performing the normalization operation on Eq. (9) produces

$$EI(\theta) = EI_0\left(\frac{F}{F_0}\right)^{a(\theta)}\left(\frac{\varphi I_S}{\varphi_0 I_{S0}}\right)^{b(\theta)}\left(\frac{\rho}{\rho_0}\right)^{c(\theta)}\left(\frac{\varphi}{\varphi_0}\right)^{d(\theta)} \tag{14}$$

where F_0, $\varphi_0 I_{S0}$, ρ_0, and φ_0 are the averaged values that can be derived from logging data for the targeted subsurface interval. In addition, EI_0 is the normalization factor that can be expressed as

$$EI_0 = F_0^{-\frac{\gamma_{sat}^2 - \gamma_{dry}^2}{2\gamma_{sat}^2}}(\varphi_0 I_{S0})^{-\frac{\gamma_{sat}^2 - 2\gamma_{dry}^2}{\gamma_{sat}^2}}\rho_0^{\frac{\gamma_{sat}^2 - \gamma_{dry}^2}{\gamma_{sat}^2}}\varphi_0^{\frac{3\gamma_{sat}^2 - 5\gamma_{dry}^2}{2\gamma_{sat}^2}} \tag{15}$$

Dividing both sides of Eq. (14) with EI_0 and taking the natural logarithm on both sides of the obtained equation can produce

$$\ln\frac{EI(\theta)}{EI_0} = a(\theta)\ln\left(\frac{F}{F_0}\right) + b(\theta)\ln\left(\frac{\varphi I_S}{\varphi_0 I_{S0}}\right) + a(\theta)\ln\left(\frac{\rho}{\rho_0}\right)$$
$$+ a(\theta)\ln\left(\frac{\varphi}{\varphi_0}\right) \tag{16}$$

Finally, the inversion framework by using different angle-stacked seismic data can be established as

$$\begin{Bmatrix} \ln[EI(\theta_1)/EI_0] \\ \ln[EI(\theta_2)/EI_0] \\ \ln[EI(\theta_3)/EI_0] \\ \ln[EI(\theta_4)/EI_0] \end{Bmatrix} = \begin{bmatrix} a(\theta_1) & b(\theta_1) & c(\theta_1) & d(\theta_1) \\ a(\theta_2) & b(\theta_2) & c(\theta_2) & d(\theta_2) \\ a(\theta_3) & b(\theta_3) & c(\theta_3) & d(\theta_3) \\ a(\theta_4) & b(\theta_4) & c(\theta_4) & d(\theta_4) \end{bmatrix}$$
$$\times \begin{bmatrix} \ln(F/F_0) \\ \ln(\varphi I_S/\varphi_0 I_{S0}) \\ \ln(\rho/\rho_0) \\ \ln(\varphi/\varphi_0) \end{bmatrix} \tag{17}$$

where θ_1, θ_2, θ_3, and θ_4 represent different incidence angles. The inversion results can be solved using the least square method.

3. Results and discussion

3.1. Accuracy analysis of the new AVO equation

As shown in Fig. 1, we analyze the weighting coefficients for the four terms in Eq. (7) for the cases of γ_{dry}^2 of 1.333, 2, and 2.333, respectively. The value of γ_{sat}^2 is set as 4. It is observed that the weighting coefficients are negative for $\Delta F/F$ and positive for $\Delta\rho/\rho$ and $\Delta\varphi/\varphi$. As the value of γ_{dry}^2 increases, the weighting coefficients for $\Delta F/F$, $\Delta\rho/\rho$, and $\Delta\varphi/\varphi$ get closer to the zero axis and the effect of γ_{dry}^2 for these terms decreases. At the same time, the weighting coefficients change from negative to positive for $\Delta(\varphi I_S)/(\varphi I_S)$.

As depicted in Fig. 2, a simple seismic model is designed to assess the accuracy of the proposed AVO equation (Eq. (7)). In this model, a gas-bearing tight sandstone layer is embedded within mudstone. The properties of both the tight sandstone and
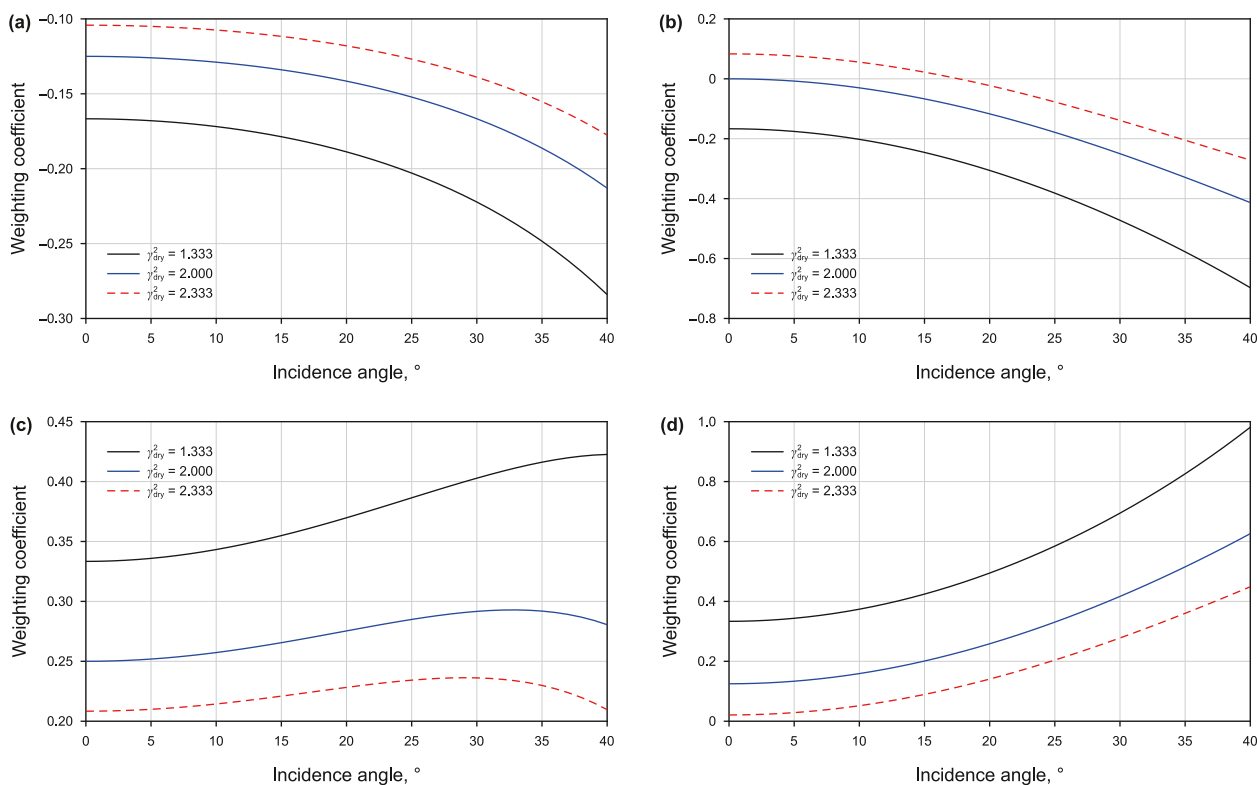
Fig. 1. Weighting coefficients for **(a)** $\Delta F/F$, **(b)** $\Delta(\varphi I_S)/(\varphi I_S)$, **(c)** $\Delta\rho/\rho$, and **(d)** $\Delta\varphi/\varphi$ of three different dry rock velocity ratio cases.
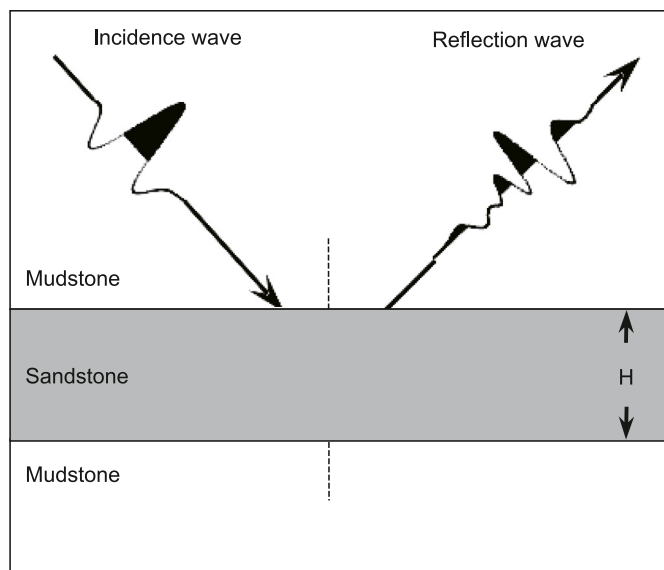
Fig. 2. Model for the calculation of seismic reflection coefficients.

Table 1
Properties used for the evaluation of the new AVO equation.

	V_P, km/s	V_S, km/s	P, g/cm³	M, GPa	S_g	φ	K_f, GPa
Mudstone	3.80	2.00	2.60	10.40	0	0.08	2.25
Sandstone	4.30	2.80	2.40	18.82	0.7	0.10	0.06

mudstone are delineated in Table 1. The tight sandstone is set to have higher values of V_P and V_S than those of the mudstone.

Furthermore, the corresponding shear wave moduli, μ, are derived from the elastic wave velocities and densities. Additionally, the tight sandstone is assumed to be partially gas-saturated ($S_g = 0.7$), while the mudstone is presumed to be completely water-saturated ($S_g = 0$). The porosities are set at 0.08 for the mudstone and 0.10 for the tight sandstone. Subsequently, the corresponding fluid bulk modulus (K_f) can be calculated utilizing Wood's equation ($K_f = [S_g/K_g + (1 - S_g)/K_w]^{-1}$) (Wood, 1941), where the bulk modulus of gas (K_g) is established as 0.04 GPa and the bulk modulus of water (K_w) is determined as 2.25 GPa.

For the properties outlined in Table 1, the PP-wave reflection coefficients (R_{PP}) are computed for the top and bottom interfaces of the tight sandstone layer, as depicted in Fig. 2. Following the approach of Russell et al. (2011), γ_{dry} is considered as an adjustable parameter. Its determination is based on yielding reasonable estimations of the reflection coefficients during modeling. Moreover, this adjustable parameter can be optimized to achieve the most effective discrimination between gas- and water-saturated reservoirs in field data applications. Russell et al. (2011) proposed a plausible range of γ_{dry} values. In this study, the value of γ_{dry} is set to 1.58, which yields a reasonable accuracy in the calculation of R_{PP} using Eq. (7).

As depicted in Fig. 3, the R_{PP} values computed using the new AVO equation (Eq. (7)) exhibit close agreement with those obtained through the Fatti approximation (Eq. (6)) and the exact Zoeppritz equations (Zoeppritz, 1919). Minor deviations are observed only at incidence angles exceeding approximately 30°. Consequently, these results substantiate the accuracy of the proposed AVO equation.

3.2. Effectiveness evaluation of the F indicator based on logging data analyses and rock physical modeling

The seismic two-way time (TWT) map of the targeted tight
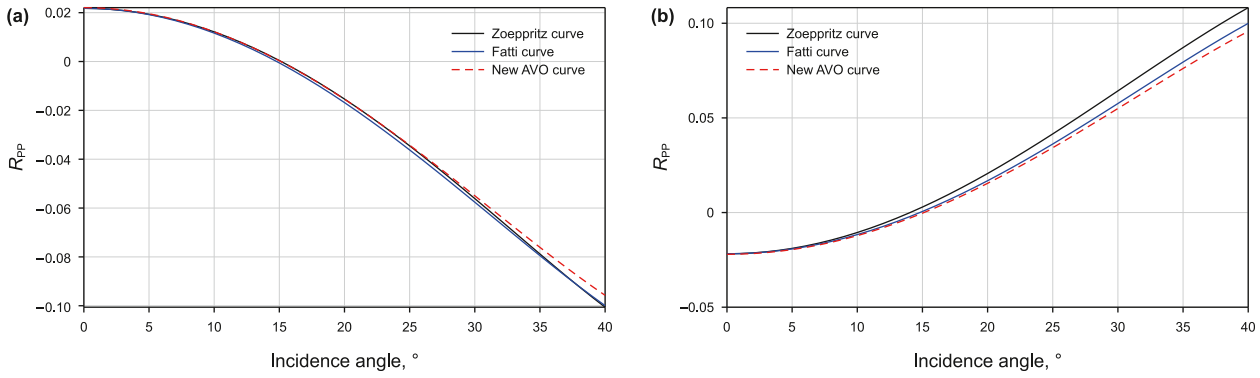
Fig. 3. Calculated R_{PP} values by using the Zoeppritz (black solid curves), the Fatti (blue solid curves), and the proposed AVO (red dashed curves) equations for the **(a)** upper and **(b)** lower interfaces of the tight sandstone layer.
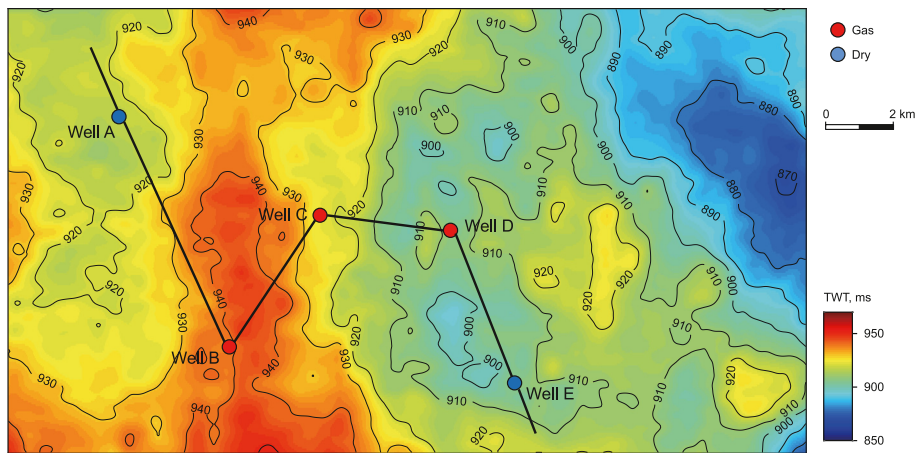
Fig. 4. Two-way travel time for the targeted tight sandstones. The red dots indicate the locations of the gas wells B, C, and D. The blue dots indicate the locations of the dry wells A and E, and the black line shows the cross-well seismic line.
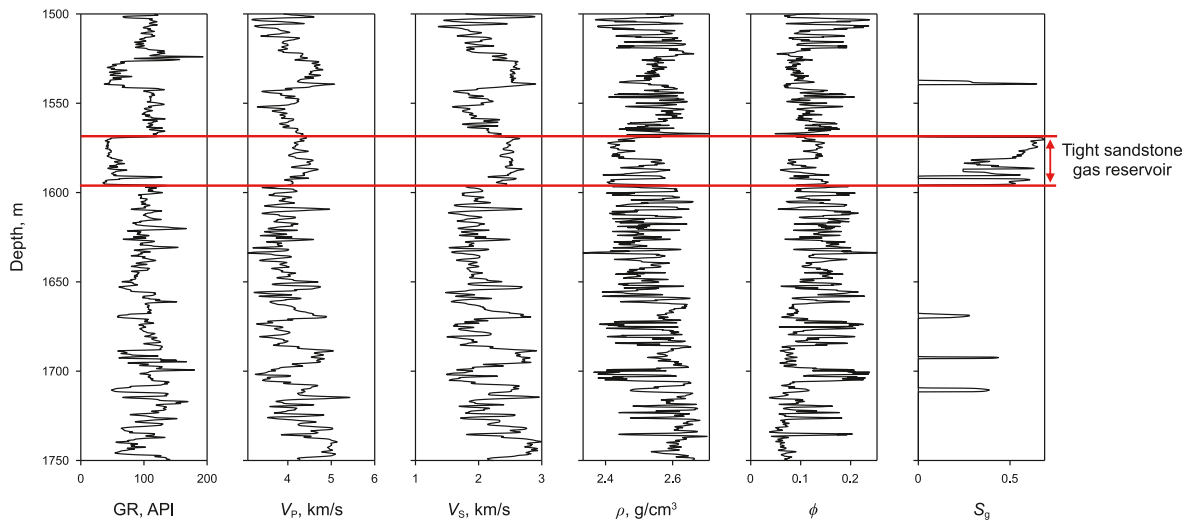
Fig. 5. Logging data including GR, V_P, V_P, ρ, φ, and S_g for well B.

sandstone (Fig. 4) depicts a relatively uniform subsurface structure of the tight formation within the studied area. Among the five designated wells A–E, wells A and E are non-productive, while wells B, C, and D yield gas. Fig. 5 illustrates the logging curves from gas-producing well B, illustrating the geological structure and

petrophysical properties of the tight formations. Gas-bearing tight sandstones are discerned by relatively low GR values, high velocities, high density, and high S_g values.

We compute K_f values using Wood's equation and well-log data obtained from the five boreholes A–E. The resulting plot of K_f
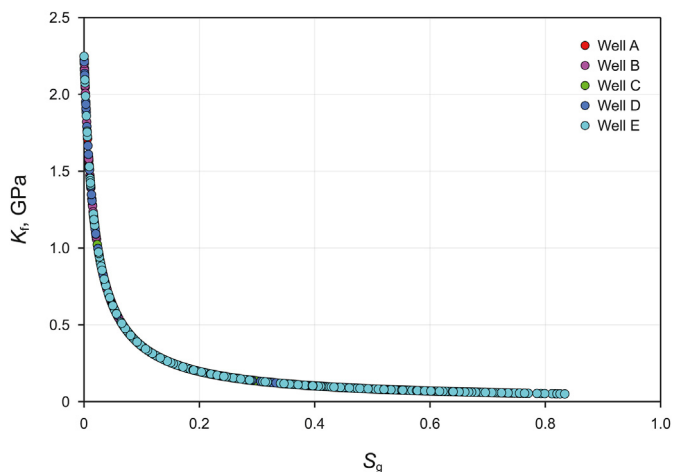
Fig. 6. Calculated K_f versus S_g for the five wells A−E.

Fig. 9. Cross-plot of S_g and φ, as color-coded by F for the five wells A−E.

versus S_g is depicted in Fig. 6. Notably, K_f exhibits a sharp decrease with increasing S_g for $S_g < 0.2$. However, for $S_g > 0.2$, K_f displays reduced sensitivity to gas saturation, indicating the limitations of K_f as a gas indicator for discriminating tight sandstones with high gas saturation. Subsequently, the F values are computed using Eq. (5) and logging data from the five wells A−E. The cross-plot of calculated F versus S_g demonstrates a positive correlation between the two factors (Fig. 7(a)). Further analysis, as depicted in Fig. 7(b), indicates that the scattering distribution of the data points is associated with porosity, with straight lines qualitatively representing constant φ lines. Additionally, the cross-plot in Fig. 8(a) reveals that the calculated F values can reflect changes in φ. However, it is observed that S_g significantly influences the relation between F and φ, as qualitatively illustrated by the constant S_g lines in
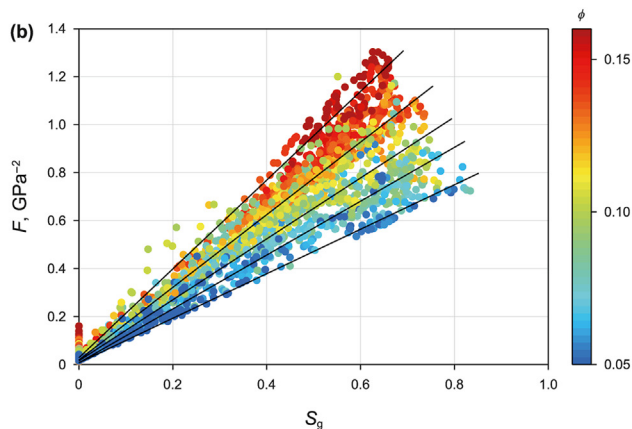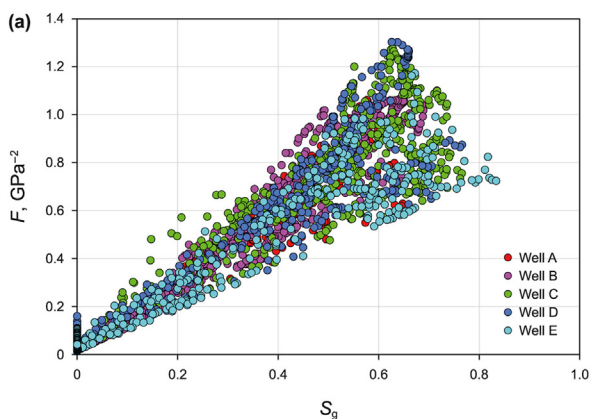
Fig. 7. **(a)** Cross-plot of S_g and calculated F for the five wells A−E, and **(b)** the same cross-plot that is color-coded by φ.
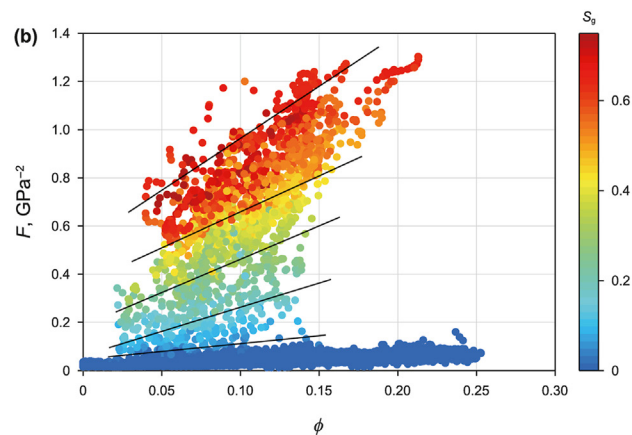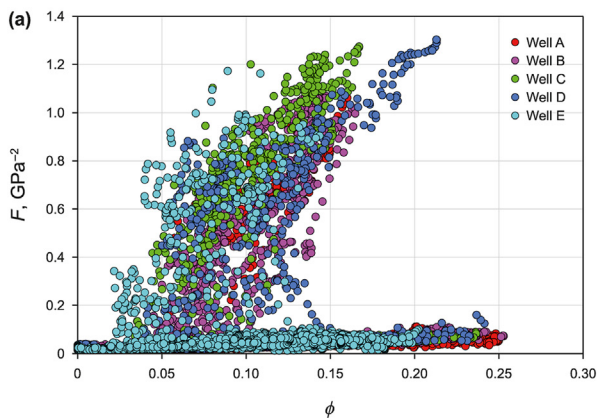
Fig. 8. **(a)** Cross-plot of φ and the calculated F for the five wells A−E, and **(b)** the same cross-plot that is color-coded by S_g.
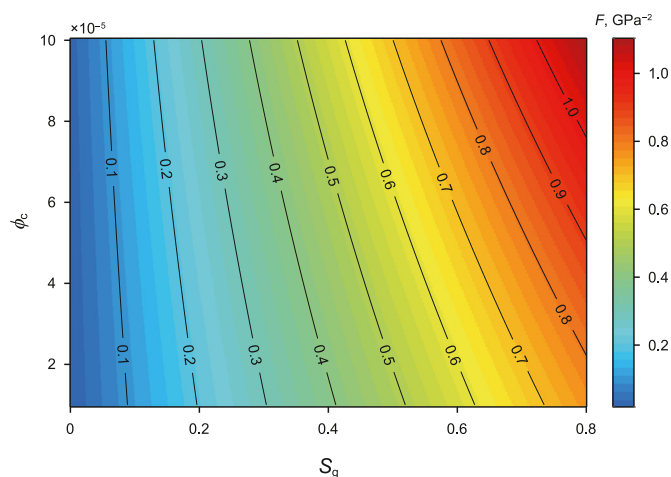
Fig. 10. Calculated F computed for varying S_g and φ by using the rock physical modeling method (Guo et al., 2021).
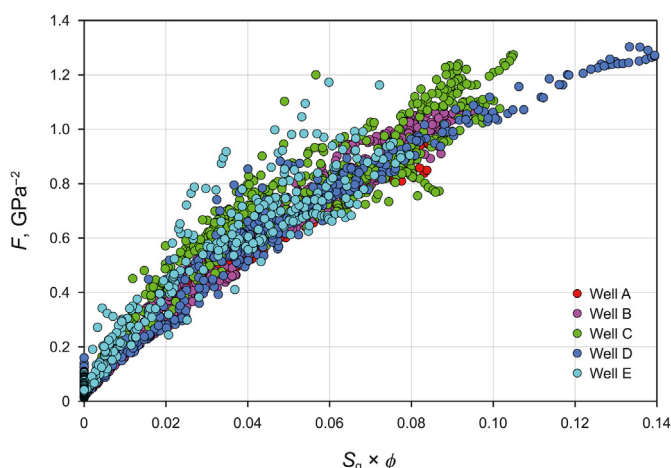
Fig. 11. Cross-plot of $S_g \times \varphi$ and calculated F for the five wells A–E.

Fig. 8(b). Thus, it is imperative to consider the comprehensive impact of both S_g and φ on the F factor.

The relationships among F, S_g, and φ are extensively examined utilizing well-log data (Fig. 9). Analysis reveals that higher values of F correlate with higher values of both S_g and φ. Additionally, employing the rock physical method proposed by Guo et al. (2021), how F values fluctuate with changes in S_g and φ is investigated. To accomplish this, the fluid and elastic properties of the tight sandstones are computed and employed to derive F across varying levels of S_g and φ. As illustrated in Fig. 10, the findings verify the trends observed in the well-log data depicted in Fig. 9. This supports the inference that F serves as a reliable indicator for both S_g and φ. Additionally, Fig. 11 presents a cross-plot of $S_g \times \varphi$ and the calculated F values for the five wells A–E. A clear positive correlation is evident between F and $S_g \times \varphi$, indicating that the F factor is effective for identifying gas content, as represented by $S_g \times \varphi$.

3.3. Real data applications

The profiles in Fig. 12 display partial angle-stacked seismic data for incidence angles of 0°, 10°, 20°, and 30° across the five wells A–E. The interpreted top and bottom horizons of the tight sandstone reservoirs are delineated by two black lines. The seismic data

is sampled at intervals of 1 ms. Subsequently, the four partial angle-stacked seismic profiles are used to derive elastic impedance for the incidence angles of 0°, 10°, 20°, and 30°, as illustrated in Fig. 13. Following the approach outlined in Section 2.2, inversion operations are subsequently conducted utilizing these elastic impedances. Furthermore, the GR logging curves for the five wells A–E are superimposed on the profiles depicted in Figs. 12 and 13.

Utilizing the method outlined in Section 2.2 and the elastic impedances illustrated in Fig. 13, the parameters F and φ can be computed, with the results depicted in Figs. 14 and 15, respectively. As indicated by the findings presented in Fig. 11, the calculated F parameter serves as an effective indicator of $S_g \times \varphi$. Consequently, the $S_g \times \varphi$ curves obtained from the logging data are overlaid in Fig. 14. It is observed that the calculated F values exhibit a favorable agreement with the $S_g \times \varphi$ values across the wellbores A–E. The calculated F values exhibit obvious anomalies in the gas-producing wells B, C, and D while demonstrating relatively weak responses in the dry wells A and E. In particular, the anomaly of the high $S_g \times \varphi$ values for the thin layers can be identified by high F values. This underscores the capability of the calculated F parameter to provide accurate estimations of gas content in tight formations. Additionally, the logging curves of φ are superimposed on the calculated profile of φ in Fig. 15. The results indicate that the seismic-inverted φ values align reasonably well with the values measured in the wellbores A–E. The difference between the findings presented in Figs. 14 and 15 is that the former incorporates the comprehensive effects of gas saturation and porosity ($S_g \times \varphi$).

In the current study, both K_f and μ values have been computed (Figs. 16 and 17), and the F values are derived from the definition $F = 1/(K_f \times \mu)$ (Fig. 18). The F values, estimated from K_f and μ using the above definition, can be compared with directly estimated values obtained through the method proposed in this study (Fig. 14).

Employing the AVO equation proposed by Yin and Zhang (2014), the K_f values are predicted through elastic impedance inversion, following a process similar to that presented in Section 2.2. The predicted K_f values are depicted in Fig. 16. Theoretically, K_f, defined as the pore fluid bulk modulus, can be utilized to estimate S_g. However, as indicated by Fig. 6, direct estimation of S_g using K_f is not feasible across the entire range of gas saturation, as K_f proves to be insensitive to gas saturation for $S_g > 0.2$. Consequently, while K_f can effectively discriminate tight sandstones with low gas saturation, its capacity to identify those with medium and high gas saturation is limited. This limitation reveals the challenges associated with accurate gas predictions in tight formations when using the K_f parameter. Furthermore, μ values (Fig. 17) can be derived from seismic-inverted elastic parameters provided in the datasets. Subsequently, the profile of $1/(K_f \times \mu)$ can be derived using the results presented in Figs. 16 and 17. According to the definition $F = 1/(K_f \times \mu)$, the results presented in Fig. 18 offer an indirect estimation of the F parameter.

Comparing the results depicted in Figs. 14 and 18, it becomes evident that directly inverted F values show better agreements with the $S_g \times \varphi$ loggings compared to the values obtained from $1/K_f \times \mu$. The predicted F values successfully identify gas zones in wells B and C within the intervals delineated by the two black solid lines. In contrast, the anomaly responses within the same gas zones in wells B and C appear weak. Particularly the high gas content in the targeted interval in well C is not well recognized in the $1/(K_f \times \mu)$ profile. Moreover, the $1/(K_f \times \mu)$ profile indicates high gas content below the targeted intervals in wells B and C. However, as indicated by the $S_g \times \varphi$ loggings, this observation could be misleading, as there are no gas indications in these deeper formations.

The effectiveness of the F parameter for gas prediction is further
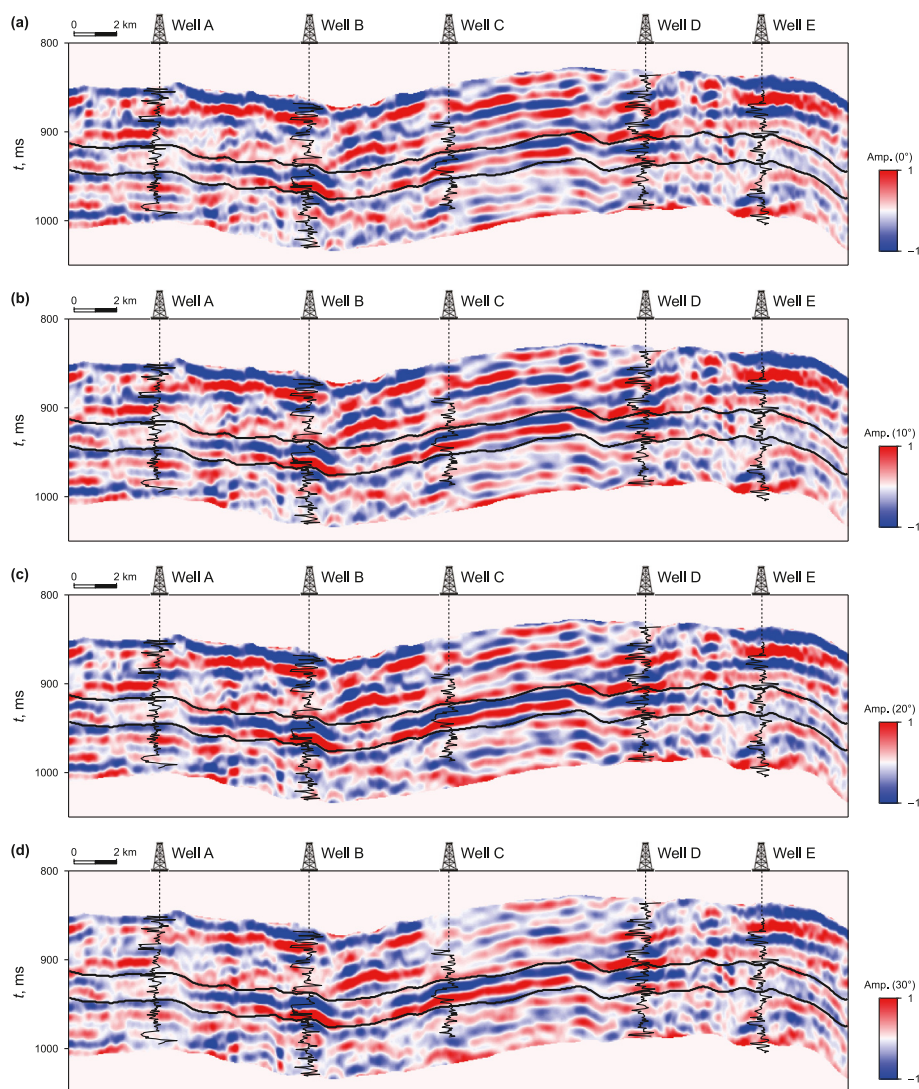
Fig. 12. Profiles of the partial angle-stacked seismic **(a)** 0°, **(b)** 10°, **(c)** 20°, and **(d)** 30°, which are superimposed by GR loggings for the five wells A-E. The interpreted top and bottom of the tight sandstone gas reservoirs are marked by two black lines. The "Amp." is the abbreviation of amplitude.

validated by its ability to reasonably identify thin gas layers in the shallower formations of wells B, D, and E. The better performance of F, in comparison to $1/(K_f \times \mu)$, in gas prediction can be explained by the fact that direct inversion of reservoir parameters would reduce cumulative errors in calculations, as discussed by Zhang et al. (2020b).

Finally, three-dimensional (3D) volumes of F and φ are depicted in Figs. 19 and 20, respectively. The calculated F values exhibit more concentrated anomaly distributions compared to the calculated φ. This can be attributed to the fact that higher F values correspond to both higher porosity and higher gas saturation in tight formations. Consequently, the obtained F parameter offers estimations of the spatial distributions of gas content (Fig. 19). Moreover, it facilitates a comprehensive characterization of tight sandstones by integrating the assessed porosity (Fig. 20) and other reservoir properties (such as brittleness and microcracks) estimated from seismic data.

4. Discussion

Identifying sweet spots with high gas enrichment represents a primary task in the exploration of tight sandstone gas reservoirs.

Evaluating gas enrichment should also consider the effect of gas saturation and porosity. To address this challenge, the factor F, formulated in terms of K_f and μ (Eq. (5)), is proposed as an indicator for gas enrichment estimation. Quantitative analyses utilizing logging data demonstrate an obvious positive correlation between F and $S_g \times \varphi$. This correlation, as depicted in Fig. 11, shows that F is an effective indicator for estimating gas enrichment.

Additionally, a new AVO equation (Eq. (7)), parameterized in terms of F, φ, and relevant elastic parameters, is proposed in this study. This equation facilitates the extraction of reservoir property information directly from prestack seismic data. Validated through the comparison of reflection coefficients calculated using the new AVO equation with those obtained from exact solutions of the Zoeppritz equations (Fig. 3), the proposed AVO equation demonstrates high accuracy. While several inversion methods can be employed by solving the objective function defined by the new AVO equation and logging data of reservoir properties, the elastic impedance approach emerges as a robust alternative for the inversion of the reservoir properties. This method effectively prevents the influence of errors in the measurement of reservoir properties, thereby enhancing the stability of the inversion. The
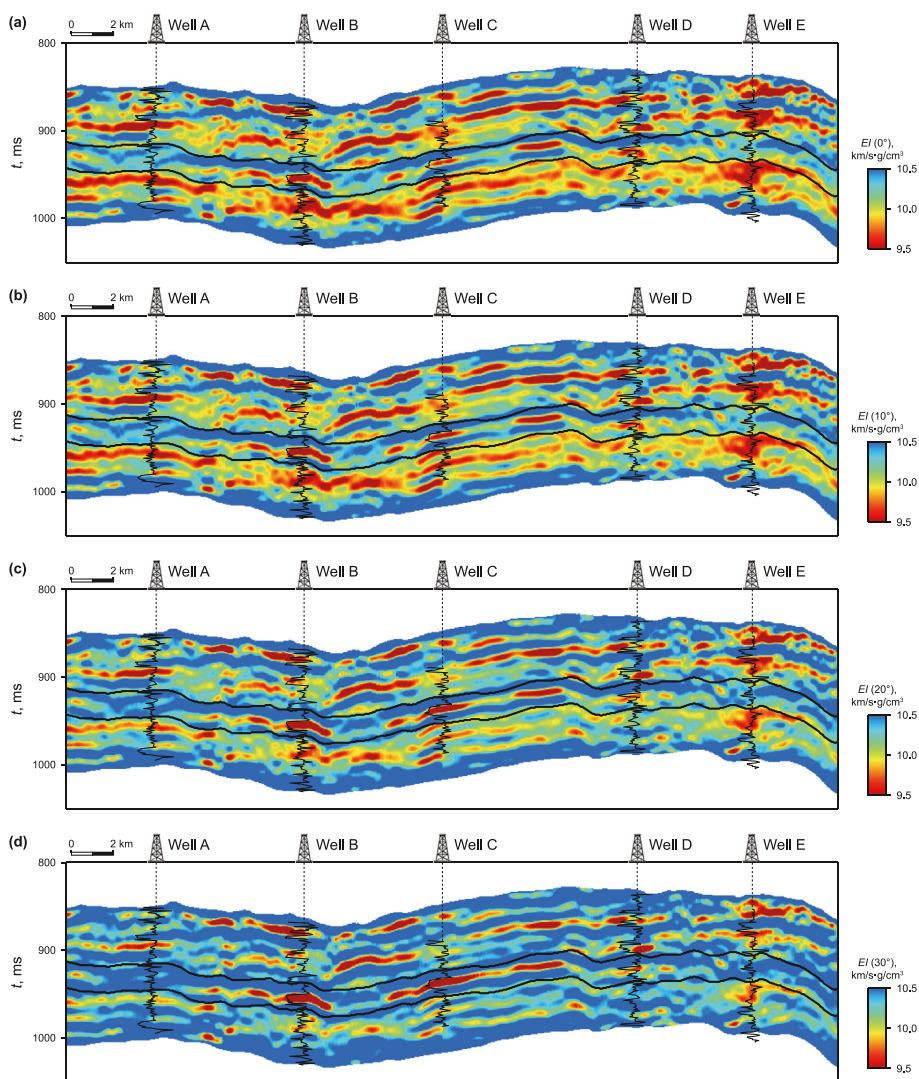
Fig. 13. Profiles of the elastic impedances (**a**) $EI(0°)$, (**b**) $EI(10°)$, (**c**) $EI(20°)$, and (**d**) $EI(30°)$, which are superimposed by GR loggings for the five wells A−E. The interpreted top and bottom of the tight sandstone gas reservoirs are marked by two black lines.
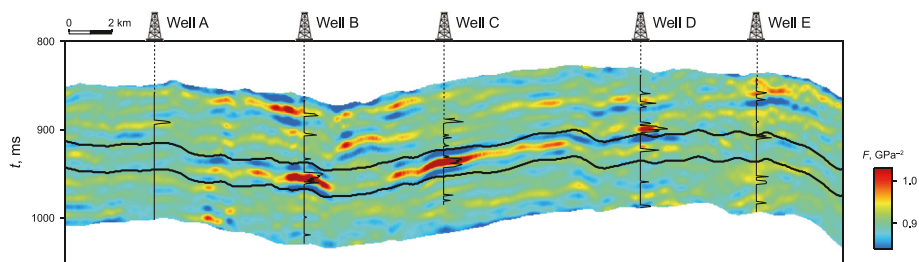
Fig. 14. Calculated profile of F, with superimposed $S_g \times \varphi$ loggings for the five wellbores A−E. The interpreted top and bottom of the tight sandstone gas reservoirs are marked by two black lines.

fundamental requirement for employing elastic impedance in prestack inversion is the reasonable accuracy of the new AVO equation, as validated in Fig. 3. Additionally, elastic impedances for various incidence angles can be obtained through routine procedures using the methods outlined by Connolly (1999) and Whitecombe et al. (2002). Consequently, the proposed AVO equation is reformulated into the elastic impedance inversion framework (Eq. (17)), enabling direct estimations of F and φ from partial

angle-stacked seismic data.

As depicted in Figs. 14 and 15, the estimated F and φ values exhibit favorable agreement with the logging data, suggesting that these parameters offer reliable predictions of the extent of high gas enrichments in tight sandstones. Additionally, another method for indirectly estimating F values (Fig. 18) has been considered, involving the calculation of both K_f and μ (Figs. 16 and 17), followed by the derivation of F using the definition $F = 1/K_f\, \mu$ (Eq. (5)). As
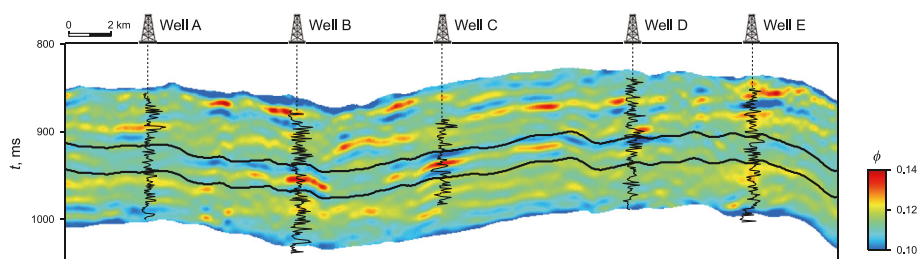
Fig. 15. Calculated profile of φ, with superimposed φ loggings for the five wellbores A−E. The interpreted top and bottom of the tight sandstone gas reservoirs are marked by two black lines.
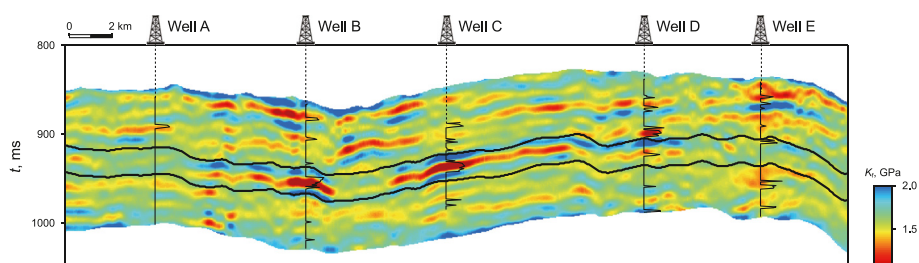
Fig. 16. Profile of K_f, superimposed by S_g loggings for the five wellbores A−E. The interpreted top and bottom of the tight sandstone gas reservoirs are marked by two black lines.
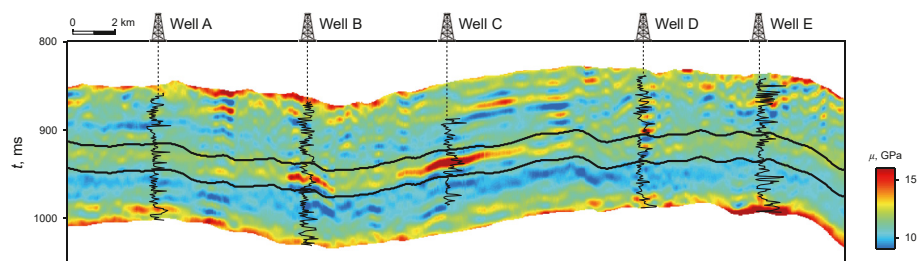
Fig. 17. Profile of μ, superimposed by GR loggings for the five wellbores A−E. The interpreted top and bottom of the tight sandstone gas reservoirs are marked by two black lines.
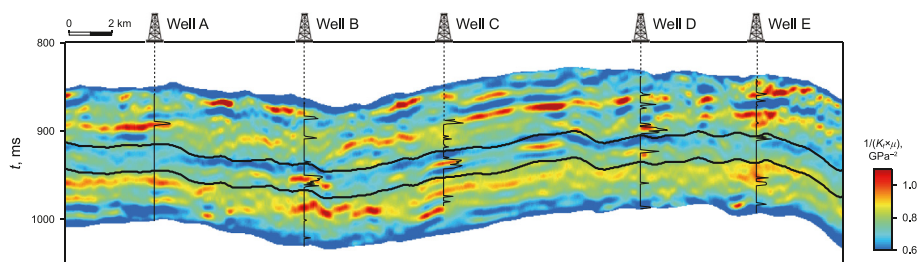
Fig. 18. Profile of $1/(K_f \times \mu)$, superimposed by $S_g \times \varphi$ loggings for the five wellbores A−E. The interpreted top and bottom of the tight sandstone gas reservoirs are marked by two black lines.

discussed in Section 3.3, the *F* factor obtained through the direct inversion method (Fig. 14) presents a more reasonable estimation of gas-bearing tight sandstones compared to the indirect method (Fig. 18). The enhanced reliability of the estimated *F* factor (Fig. 14) can be explained by the fact that the direct inversion procedure would reduce cumulative errors in calculations (Zhang et al., 2020b).

In conclusion, the computed 3D volumes of *F* and φ values (Figs. 19 and 20) have provided essential information about the reservoir properties for the identification of sweet spots in tight sandstone reservoirs. However, while the proposed method has

been successfully applied for reservoir property estimations, it is important to note that different effective reservoir parameters can be explored based on logging data analyses and rock physical modeling, especially for other hydrocarbon reservoirs.

5. Conclusions

In this study, a new AVO equation parameterized by indicators of gas content, porosity, and relevant elastic parameters has been proposed. This equation enables the direct extraction of reservoir properties from prestack seismic data for tight gas sandstones. The
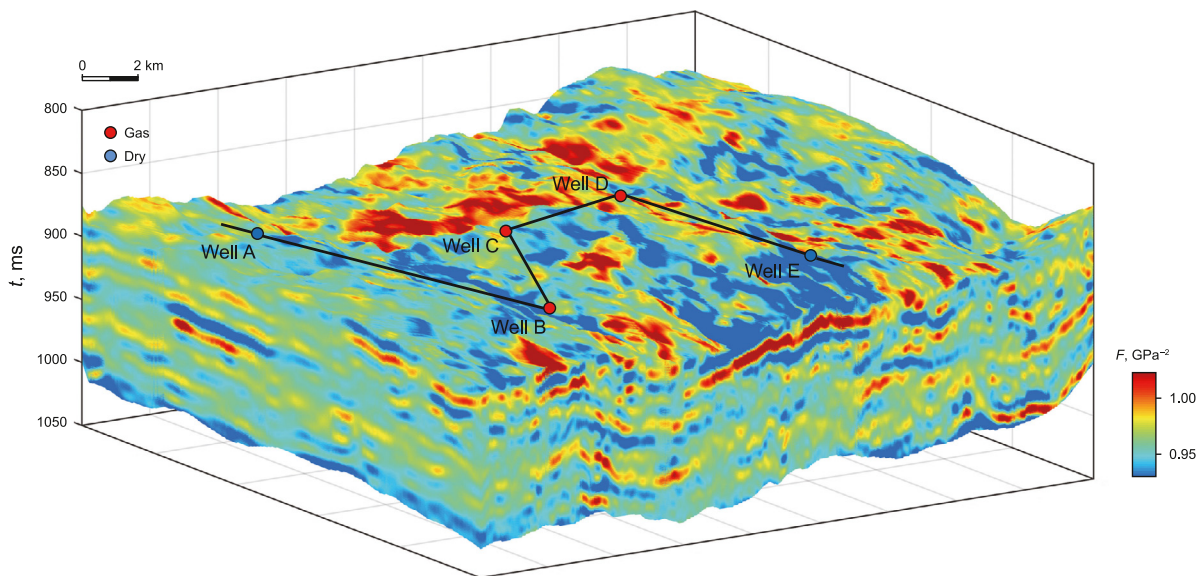
Fig. 19. 3D volume of the F parameter for the studied area with the five wellbores A—E.
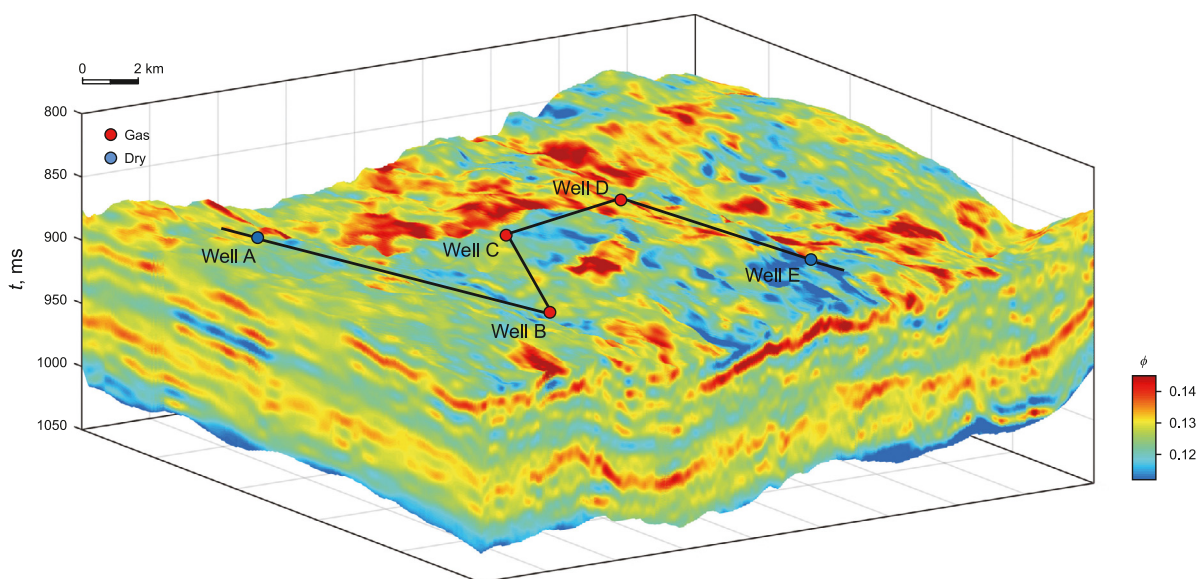
Fig. 20. 3D volume of the φ parameter for the studied area with the five wellbores A—E.

proposed gas content indicator, formulated in terms of effective fluid bulk modulus and shear modulus, exhibits an evident positive correlation with gas content based on logging data analyses. Comparisons demonstrate that it can achieve a reasonable accuracy with the proposed AVO equation compared to the exact resolutions provided by the Zoeppritz equation. An elastic impedance inversion approach is developed utilizing the proposed AVO equation. The purpose of this inversion method is to enable robust estimations of reservoir properties from prestack seismic data. Additionally, the estimated gas content indicator and porosity demonstrate good agreement with logging data, suggesting that these parameters offer reliable predictions of high gas enrichment in tight sandstones. The methods presented in this study may serve as inspiration for the development of other direct estimation methods for various types of hydrocarbon resources and properties.

CRediT authorship contribution statement

Han Jin: Writing — original draft, Visualization, Software, Methodology, Investigation, Formal analysis, Data curation. **Cai Liu:** Supervision, Resources. **Zhi-Qi Guo:** Writing — review & editing, Writing — original draft, Visualization, Validation, Resources, Project administration, Methodology, Investigation, Formal analysis, Conceptualization.

Declaration of competing interest

The authors declare that they have no known competing financial interests or personal relationships that could have appeared to influence the work reported in this paper.

Acknowledgments

Appendix A. Establishment of the new AVO equation

Murphy et al. (1991) proposed the formulas of velocities based on Gassmann's equation:

$$\rho V_P^2 = K_{dry} + \frac{4}{3}\mu + f \tag{A.1}$$

$$\rho V_S^2 = \mu \tag{A.2}$$

$$f = \frac{\left(1 - \frac{K_{dry}}{K_s}\right)^2}{\frac{\varphi}{K_f} + \frac{1-\varphi}{K_s} - \frac{K_{dry}}{K_s^2}} \tag{A.3}$$

where V_P, V_S, and ρ represent the compressional wave velocity, shear wave velocity, and density, respectively, of the saturated rock. Also, K_{dry} denotes the bulk modulus of the dry rock, μ signifies the shear modulus of the rock skeleton, K_s stands for the bulk modulus of the solid grain, K_f represents the fluid bulk modulus, φ is the porosity, and f represents the fluid/porosity term.

On the other hand, Russell et al. (2011) presented

$$\gamma_{dry}^2 = \frac{K_{dry}}{\mu} + \frac{4}{3} \tag{A.4}$$

$$\gamma_{sat} = \left(\frac{V_P}{V_S}\right)_{sat} \tag{A.5}$$

Multiplying both sides of Eq. (A.4) by μ and then substituting Eq. (A.2) into the resulting formula yields

$$\gamma_{dry}^2 \rho V_S^2 = K_{dry} + \frac{4}{3}\mu \tag{A.6}$$

Further, combining Eq. (A.6) and Eq. (A.1) produces

$$f = \rho V_P^2 - \gamma_{dry}^2 \rho V_S^2 \tag{A.7}$$

Dividing both sides of Eq. (A.7) with ρV_P^2 and incorporating the expression in Eq. (A.5) generate

$$\frac{f}{\rho V_P^2} = \frac{\rho V_P^2 - \gamma_{dry}^2 \rho V_S^2}{\rho V_P^2} = 1 - \frac{\gamma_{dry}^2}{\gamma_{sat}^2} \tag{A.8}$$

Eq. (A.8) can be reformulated by employing the definition $I_P = \rho V_P$:

$$I_P = \frac{f}{V_P\left(1 - \frac{\gamma_{dry}^2}{\gamma_{sat}^2}\right)} \tag{A.9}$$

Multiplying both sides of Eq. (A.9) by μ and using the simplified form of the fluid/porosity term f provided by Han and Batzle (2003):

$$f = K_f G(\varphi) \tag{A.10}$$

where $G(\varphi) = \frac{(1-K_{dry}/K_s)^2}{\varphi}$, and K_s is the bulk modulus of the solid grain.

Eq. (A.9) can be further expressed as

$$I_P \mu = \frac{K_f \mu G(\varphi)}{V_P\left(1 - \frac{\gamma_{dry}^2}{\gamma_{sat}^2}\right)} \tag{A.11}$$

After multiplying $\rho^2 V_P(1 - \gamma_{dry}^2/\gamma_{sat}^2)$ on both sides of Eq. (A.11) and by defining the factor F in Eq. (A.12):

$$F = \frac{1}{K_f \mu} \tag{A.12}$$

Eq. (A.11) can be reorganized as

$$I_P \mu \rho^2 V_P\left(1 - \frac{\gamma_{dry}^2}{\gamma_{sat}^2}\right) = \frac{G(\varphi)\rho^2}{F} \tag{A.13}$$

Based on the analysis of well-log data, the proposed F parameter demonstrates strong agreement with gas content, defined as the product of porosity (φ) and gas saturation (S_g) (as elaborated above). Thus, the proposed F parameter can serve as an effective indicator of gas content for characterizing tight sandstones.

Based on the relation:

$$\gamma_{sat} = \left(\frac{V_P}{V_S}\right)_{sat} = \left(\frac{I_P}{I_S}\right)_{sat} \tag{A.14}$$

and the expression $I_S^2 = \mu\rho$, Eq. (A.13) can be reformulated as

$$I_P^2 I_S^2 - \gamma_{dry}^2 I_S^4 = \frac{G(\varphi)\rho^2}{F} \tag{A.15}$$

By defining

$$A = I_P^2 I_S^2 - \gamma_{dry}^2 I_S^4 \tag{A.16}$$

and

$$B = \frac{G(\varphi)\rho^2}{F} \tag{A.17}$$

The differences in values A and B across a subsurface interface can be obtained using the chain rule of multi-variable calculus applied to Eqs. (A.16) and (A.17):

$$\Delta A = \frac{\partial A}{\partial I_P}\Delta I_P + \frac{\partial A}{\partial I_S}\Delta I_S \tag{A.18}$$

$$\Delta B = \frac{\partial B}{\partial G(\varphi)}\Delta G(\varphi) + \frac{\partial B}{\partial \rho}\Delta\rho + \frac{\partial B}{\partial F}\Delta F \tag{A.19}$$

Also, substituting Eq. (A.16) into Eq. (A.18) produces

$$\Delta A = 2I_P I_S^2 \Delta I_P + \left(2I_P^2 I_S - 4\gamma_{dry}^2 I_S^3\right)\Delta I_S \tag{A.20}$$

Furthermore, by considering the expression of A in Eq. (A.16) and the relation $I_P = I_S \gamma_{sat}$ that can be obtained from Eq. (A.14), the following expression can be obtained:

$$\frac{\Delta A}{A} = \frac{2\gamma_{sat}^2}{\gamma_{sat}^2 - \gamma_{dry}^2}\frac{\Delta I_P}{I_P} + \frac{2\gamma_{sat}^2 - 4\gamma_{dry}^2}{\gamma_{sat}^2 - \gamma_{dry}^2}\frac{\Delta I_S}{I_S} \tag{A.21}$$

In addition, substituting Eq. (A.17) into Eq. (A.19) produces

$$\Delta B = -\frac{G(\varphi)\rho^2 \Delta F}{F^2} + \frac{\rho^2 \Delta G(\varphi)}{F} + \frac{2\rho G(\varphi)\Delta\rho}{F} \qquad (A.22)$$

Then, the term $\Delta B/B$ can be obtained from Eqs. (A.17) and (A.22):

$$\frac{\Delta B}{B} = -\frac{\Delta F}{F} + \frac{\Delta G(\varphi)}{G(\varphi)} + 2\frac{\Delta\rho}{\rho} \qquad (A.23)$$

According to the results of Yin and Zhang (2014):

$$R_{PP}(\theta) = \frac{(1+\tan^2\theta)\left(\gamma_{sat}^2 - \gamma_{dry}^2\right)}{4\gamma_{sat}^2}\left(-\frac{\Delta F}{F} + \frac{\Delta\varphi}{\varphi}\right) - \frac{(1+\tan^2\theta)\left(\gamma_{sat}^2 - 2\gamma_{dry}^2\right)}{2\gamma_{sat}^2}\frac{\Delta I_S}{I_S} - \frac{4\sin^2\theta}{\gamma_{sat}^2}\frac{\Delta I_S}{I_S}$$
$$+\frac{(1+\tan^2\theta)\left(\gamma_{sat}^2 - \gamma_{dry}^2\right)}{2\gamma_{sat}^2}\frac{\Delta\rho}{\rho} - \left(\frac{\tan^2\theta}{2} - \frac{2\sin^2\theta}{\gamma_{sat}^2}\right)\frac{\Delta\rho}{\rho} \qquad (A.29)$$

Eq. (A.29) can be further reformulated as

$$R_{PP}(\theta) = -\frac{(1+\tan^2\theta)\left(\gamma_{sat}^2 - \gamma_{dry}^2\right)}{4\gamma_{sat}^2}\frac{\Delta F}{F} - \frac{(1+\tan^2\theta)\left(\gamma_{sat}^2 - 2\gamma_{dry}^2\right) + 8\sin^2\theta}{2\gamma_{sat}^2}\frac{\Delta(\varphi I_S)}{\varphi I_S}$$
$$+\left[\frac{(1+\tan^2\theta)\left(\gamma_{sat}^2 - \gamma_{dry}^2\right) + 4\sin^2\theta}{2\gamma_{sat}^2} - \frac{\tan^2\theta}{2}\right]\frac{\Delta\rho}{\rho}$$
$$+\frac{(1+\tan^2\theta)\left(3\gamma_{sat}^2 - 5\gamma_{dry}^2\right) + 16\sin^2\theta}{4\gamma_{sat}^2}\frac{\Delta\varphi}{\varphi} \qquad (A.30)$$

$$\frac{\Delta G(\varphi)}{G(\varphi)} = \frac{\Delta\varphi}{\varphi} \qquad (A.24)$$

Eq. (A.23) can be reformulated as

$$\frac{\Delta B}{B} = -\frac{\Delta F}{F} + \frac{\Delta\varphi}{\varphi} + 2\frac{\Delta\rho}{\rho} \qquad (A.25)$$

For $A = B \neq 0$, we can reasonably assume $\Delta A = \Delta B$ and further have $\Delta A/A = \Delta B/B$. Therefore, combining Eqs. (A.21) and (A.25) gives

$$\frac{2\gamma_{sat}^2}{\gamma_{sat}^2 - \gamma_{dry}^2}\frac{\Delta I_P}{I_P} + \frac{2\gamma_{sat}^2 - 4\gamma_{dry}^2}{\gamma_{sat}^2 - \gamma_{dry}^2}\frac{\Delta I_S}{I_S} = -\frac{\Delta F}{F} + \frac{\Delta\varphi}{\varphi} + 2\frac{\Delta\rho}{\rho} \qquad (A.26)$$

which can be further reorganized as

$$\frac{\Delta I_P}{I_P} = \frac{\gamma_{sat}^2 - \gamma_{dry}^2}{2\gamma_{sat}^2}\left(-\frac{\Delta F}{F} + \frac{\Delta\varphi}{\varphi} + 2\frac{\Delta\rho}{\rho}\right) - \frac{\gamma_{sat}^2 - 2\gamma_{dry}^2}{\gamma_{sat}^2}\frac{\Delta I_S}{I_S} \qquad (A.27)$$

Substituting Eq. (A.27) into Fatti's P-wave reflection coefficient equation (Fatti et al., 1994)

$$R_{PP}(\theta) = \frac{(1+\tan^2\theta)}{2}\frac{\Delta I_P}{I_P} - \frac{4}{\gamma_{sat}^2}\sin^2\theta\frac{\Delta I_S}{I_S} - \left(\frac{\tan^2\theta}{2}\right.$$
$$\left. - \frac{2}{\gamma_{sat}^2}\sin^2\theta\right)\frac{\Delta\rho}{\rho} \qquad (A.28)$$

can produce

In this newly developed AVO equation, $R_{PP}(\theta)$ is parameterized by the reflectivity terms $\Delta F/F$, $\Delta(\varphi I_S)/(\varphi I_S)$, $\Delta\rho/\rho$, and $\Delta\varphi/\varphi$. Eq. (A.30) provides a method for direct estimations of reservoir properties (such as gas content indicator F and porosity φ) using prestack seismic data.

References

Chen, F.B., Zong, Z.Y., 2022. PP wave reflection coefficient in stress-induced aniso-tropic media and amplitude variation with incident angle and azimuth inver-sion. Geophysics 87, C155–C172. https://doi.org/10.1190/geo2021-0706.1.

Chen, F.B., Zong, Z.Y., Yang, Y.M., Gu, X.Y., 2022. Amplitude-variation-with-offset inversion using P- to S-wave velocity ratio and P-wave velocity. Geophysics 87, N63–N74. https://doi.org/10.1190/geo2021-0623.1.

Chen, F.B., Zong, Z.Y., Yin, X.Y., Yang, Z.F., Yan, X.F., 2023a. Pressure and frequency dependence of elastic moduli of fluid-saturated dual-porosity rocks. Geophys. Prospect. 71. https://doi.org/10.1111/1365-2478.13395.

Chen, F.B., Zong, Z.Y., Yin, X.Y., 2023b. Pressure impacts on the wave dispersion in fluid-saturated dual-porosity media. 84th EAGE meeting Vienna Ausxtria. https://doi.org/10.1111/1365-2478.13395.

Connolly, P., 1999. Elastic impedance. Lead. Edge 18, 438–452. https://doi.org/10.1190/1.1438307.

Cui, H.Y., Zhong, N.N., Li, J., Wang, D.L., Li, Z.S., Hao, A.S., Liang, F., 2017. Study on the lower limits of petrophysical parameters of the Upper Paleozoic tight sandstone gas reservoirs in the Ordos Basin, China. Journal of Natural Gas Geoscience 2, 21–28. https://doi.org/10.1016/j.jnggs.2017.03.003.

Fatti, J.L., Smith, G.C., Vail, P.J., Strauss, P.J., Levitt, P.R., 1994. Detection of gas in sandstone reservoirs using AVO analysis: a 3-D seismic case history using the Geostack technique. Geophysics 59, 1362–1376. https://doi.org/10.1190/1.1443695.

Gao, G., Yang, Y.H., Zhao, B., Duan, H.L., Wang, X.Y., Wei, Y.Z., 2019. A method for

establishing and directly extracting sensitive identification factors of unconsolidated sandstones. Oil Geophys. Prospect. 54. https://doi.org/10.13810/j.cnki.issn.1000-7210.2019.06.017 (in Chinese).

Glubokovskikh, S., Gurevich, B., Saxena, N., 2016. A dual-porosity scheme for fluid/solid substitution. Geophys. Prospect. 64, 1112–1121. https://doi.org/10.1111/1365-2478.12389.

Goodway, W.N., Chen, T., Downton, J., 1997. Improved AVO fluid detection and lithology discrimination using Lamé petrophysical parameters; "λρ," μρ, λ/μ fluid stack," from P and S inversions. In: 67th Annual International Meeting SEG Expanded Abstracts, pp. 183–186. https://doi.org/10.1190/1.1885795.

Guo, Z.Q., Qin, X.Y., Zhang, Y.M., Niu, C., Wang, D., Ling, Y., 2021. Numerical investigation of the effect of heterogeneous pore structures on elastic properties of tight gas sandstones. Front. Earth Sci. 9, 641637. https://doi.org/10.3389/feart.2021.641637.

Guo, Q., Ba, J., Carcione, J.M., 2022. Multi-Objective petrophysical seismic inversion based on the double-porosity Biot-Rayleigh model. Surv. Geophys. 43, 1117–1141. https://doi.org/10.1007/s10712-022-09692-6.

Gurevich, B., Brajanovski, M., Galvin, R.J., Müller, T.M., Toms-Stewart, J., 2009. P-wave dispersion and attenuation in fractured and porous reservoirs − poroelasticity approach. Geophys. Prospect. 57, 225–237. https://doi.org/10.1111/j.1365-2478.2009.00785.x.

Han, D., Batzle, M., 2003. Gain function and hydrocarbon indicators. In: 73rd annual international meeting. SEG Expanded Abstracts, 1695–1698. https://doi.org/10.1190/1.1817633.

Huang, X.R., Huang, J.P., Li, Z.C., 2015. High-sensitivity fluid identification factor in anisotropic tight-oil sandstone reservoirs. SEG Annual Meeting, 2688–2692. https://doi.org/10.1190/segam2015-5909080.1.

Jia, L.Y., Li, L., Wang, Q.Y., Ma, J.F., Wang, H.F., Wang, D.X., 2018. Fluid identification factor inversion based on generalized elastic impedance. Geophys. Prospect. Pet. 57, 302–311. https://doi.org/10.3969/j.issn.1000-1441.2018.02.016 (in Chinese).

Li, D.Q., Wei, J.X., Di, B.R., Ding, P.B., Shuai, D., 2017. The effect of fluid saturation on the dynamic shear modulus of tight sandstones. J. Geophys. Eng. 14, 1072–1086. https://doi.org/10.1088/1742-2140/aa7179.

Liu, L., Tang, D.Z., Wo, Y.J., Liu, L.H., Sun, W., Lu, H.M., Yekikang, M.Q., 2019. Favorable area prediction of tight sandstone: a case study of the He8 formation in the Kangning area, Eastern Ordos Basin, China. J. Pet. Sci. Eng. 175, 430–443. https://doi.org/10.1016/j.petrol.2018.12.069.

Ma, Z.Q., Yin, X.Y., Zong, Z.Y., Tan, Y.Y., Ji, L.X., Yang, Z.F., Yan, X.F., 2023. Sequential Bayesian seismic inversion for fracture parameters and fluid indicator in tilted transversely isotropic media. Geophysics 88, R355–R371. https://doi.org/10.1190/geo2022-0439.1.

Murphy, W.F., Schwartz, L.M., Hornby, B., 1991. Interpretation physics of V_P and V_S in sedimentary rocks. In: Transactions SPWLA 32nd Annual Logging Symposium, pp.1–24.

Quakenbush, M., Shang, B., Tuttle, C., 2006. Poisson impedance. Lead. Edge 25, 128–138. https://doi.org/10.1190/1.2172301.

Ren, J.H., Zhang, L., Ezekiel, J., Ren, S.R., Meng, S.Z., 2014. Reservoir characteristics and productivity analysis of tight sand gas in Upper Paleozoic Ordos Basin China. J. Nat. Gas Sci. Eng. 19, 244–250. https://doi.org/10.1016/j.jngse.2014.05.014.

Russell, B.H., Hedlin, K., Hilterman, F.J., Lines, L., 2003. Fluid-property discrimination with AVO: a Biot-Gassmann perspective. Geophysics 68, 29–39. https://doi.org/10.1190/1.1543192.

Russell, B.H., Gray, D., Hampson, D.P., Lines, L.R., 2006. Linearized AVO and poroelasticity. CREWES Research Report 18, 1–25.

Russell, B.H., Gray, D., Hampson, D.P., 2011. Linearized AVO and poroelasticity. Geophysics 76, 19–29. https://doi.org/10.1190/1.3555082.

Shu, Y., Sang, S.X., Lin, Y.X., Zhou, X.Z., Wang, H., Wang, Z.L., 2021. The influence of magmatic-hydrothermal activities on porosity and permeability of sandstone reservoirs in the Linxing area, Ordos Basin, Northern China. J. Asian Earth Sci. 213, 104741. https://doi.org/10.1016/j.jseaes.2021.104741.

Smith, G.C., Gidlow, P.M., 1987. Weighted stacking for rock property estimation and detection of gas. Geophys. Prospect. 35, 993–1014. https://doi.org/10.1111/j.1365-2478.1987.tb00856.x.

Wang, P., Li, J.Y., Chen, X.H., Wang, B.F., 2020. Joint probabilistic fluid discrimination of tight sandstone reservoirs based on Bayes discriminant and deterministic rock physics modeling. J. Petrol. Sci. Eng. 191, 107218. https://doi.org/10.1016/j.petrol.2020.107218.

Wang, P., Chen, X.H., Li, X.Y., Cui, Y.A., Li, J.Y., Wang, B.F., 2022. Analysis and estimation of an inclusion-based effective fluid modulus for tight gas-bearing sandstone reservoirs. IEEE Trans. Geosci. Rem. Sens. 60, 4502710. https://doi.org/10.1109/TGRS.2021.3099134.

Whitecombe, D.N., Connolly, P.A., Reagan, R.L., Redshaw, T.C., 2002. Extended elastic impedance for fluid and lithology prediction. Geophysics 67, 63–67. https://doi.org/10.1190/1.1451337.

Wood, A.B., 1941. A Textbook of Sound G. Bell and Sons, Ltd., London, OH, USA.

Xu, C.X., Ma, P.S., Lai, L.B., Sun, Y.H., Li, Z.C., 2014. Sensitivity parameters of tight sand gas: a case study of Lower Cretaceous Yingcheng Formation of Yingtai gas field in Songliao Basin, NE China. Petrol. Explor. Dev. 41, 712–716. https://doi.org/10.1016/S1876-3804(14)60092-6 (in Chinese).

Yin, X.Y., Zhang, S.X., 2014. Bayesian inversion for effective pore-fluid bulk modulus based on fluid-matrix decoupled amplitude variation with offset approximation. Geophysics 79, R221–R232. https://doi.org/10.1190/geo2013-0372.1.

Yin, X.Y., Zhang, S.X., Zhang, F., 2013. Two-term elastic impedance inversion and Russell fluid factor direct estimation method for deep reservoir fluid identification. Chin. J. Geophys. 7, 2378–2390. https://doi.org/10.6038/cjg20130724 (in Chinese).

Yin, H.J., Zhao, J.G., Tang, G.Y., Zhao, L.M., Ma, X.Y., Wang, S.X., 2017. Pressure and fluid effect on frequency-dependent elastic moduli in fully saturated tight sandstone. Journal of Geophysical Research. Solid Earth 122, 8925–8942. https://doi.org/10.1002/2017JB014244.

Zhang, M.Z., 2016. Identification method for oil-gas reservoirs based on fluid elastic impedance inversion. Prog. Geophys. 31, 2717–2723 (in Chinese).

Zhang, S.X., Yin, X.Y., Zhang, F.C., 2010. Quasi fluid modulus for delicate lithology and fluid discrimination. In: 80th Annual International Meeting. SEG, Expanded Abstracts, pp. 404–408. https://doi.org/10.1190/1.3513704.

Zhang, S., Huang, H.D., Dong, Y.P., Yang, X., Wang, C., Luo, Y.N., 2017. Direct estimation of the fluid properties and brittleness via elastic impedance inversion for predicting sweet spots and the fracturing area in the unconventional reservoir. J. Nat. Gas Sci. Eng. 45, 415–427. https://doi.org/10.1016/j.jngse.2017.04.028.

Zhang, Y., Li, J., Hou, Z.Q., 2020a. Methods of high sensitive hydrocarbon detecting based on pre-elastic information extracted directly. Prog. Geophys. 3, 1187–1195. https://doi.org/10.6038/pg2021EE0136 (in Chinese).

Zhang, F.C., Yang, J.Y., Li, C.H., Li, D., Gao, Y., 2020b. Direct inversion for reservoir parameters from prestack seismic data. J. Geophys. Eng. 17, 993–1004. https://doi.org/10.1093/jge/gxaa058.

Zoeppritz, K., 1919. Erdbebenwellen VIIIB, Über Reflexion und Durchgang seismischer Wellen durch Unstetigkeitsflächen. Göttinger Nachrichten I, 66–84 (in German).

Zong, Z.Y., Yin, X.Y., 2017. Direct inversion of Young's and Poisson impedances for fluid discrimination. Geofluids 16, 1006–1016. https://doi.org/10.1111/gfl.12202.

Zong, Z.Y., Yin, X.Y., Wu, G.C., 2012. Fluid identification method based on compressional and shear modulus direct inversion. Chin. J. Geophys. 1, 284–292. https://doi.org/10.6038/j.issn.0001-5733.2012.01.028 (in Chinese).

Zong, Z.Y., Yin, X.Y., Wu, G.C., 2015. Geofluid discrimination incorporating poroelasticity and seismic reflection inversion. Surv. Geophys. 36, 659–681. https://doi.org/10.1007/s10712-015-9330-6.